Probing Permanent Dipole Moments and Removing Exciton Fine Structures in Single Perovskite Nanocrystals by an Electric Field

Bihu Lv,[1,*] Tianyuan Zhu,[1,*] Ying Tang,[1,*] Yan Lv,[1] Chunfeng Zhang,[1] Xiaoyong Wang,[1,†] Dajun Shu,[1,‡] and Min Xiao[1,2,§]

[1]National Laboratory of Solid State Microstructures, School of Physics, and Collaborative Innovation Center of Advanced Microstructures, Nanjing University, Nanjing 210093, China

[2]Department of Physics, University of Arkansas, Fayetteville, Arkansas 72701, USA

(Received 7 May 2020; revised 27 September 2020; accepted 8 April 2021; published 10 May 2021)

Single perovskite nanocrystals have emerged as a novel type of semiconductor nanostructure capable of emitting single photons with rich exciton species and fine energy-level structures. Here we focus on single excitons and biexcitons in single perovskite $CsPbI_3$ nanocrystals to show, for the first time, how their optical properties are modulated by an external electric field at the cryogenic temperature. The electric field can cause a blueshift in the photoluminescence peak of single excitons, from which the existence of a permanent dipole moment can be deduced. Meanwhile, the fine energy-level structures of single excitons and biexcitons in a single $CsPbI_3$ nanocrystal can be simultaneously eliminated, thus preparing a potent platform for the potential generation of polarization-entangled photon pairs.

DOI: 10.1103/PhysRevLett.126.197403

In the quantum-confined Stark effect (QCSE) of semiconductor nanostructures, the overlap of electron-hole wave functions can be effectively modified by an external electric field to induce significant changes in the exciton recombination energy, oscillator strength, and radiative lifetime [1–3]. For epitaxially grown self-assembled quantum dots (QDs), the QCSE has been widely employed to remove the exciton fine-structure splittings for the generation of polarization-entangled photon pairs [4–6]. In the case of chemically synthesized colloidal nanocrystals (NCs), the QCSE is normally manifested in heterogeneous or asymmetric structures with a weak quantum confinement [7], such as nanorod, nanowire, and nanoplatelet [8–18]. The QCSE-related studies performed so far on traditional colloidal CdSe NCs have proved the powerfulness of external electric fields in tuning the absorption and emission properties [8–11], thus fostering a variety of classical applications in electro-optical modulator-switcher [12,13], charge-voltage sensing [14–16], optical memory [17], and bioimaging [18].

Very recently, a novel type of colloidal NCs with the perovskite structures has been successfully synthesized, which can reach the weak quantum-confinement regime with the side lengths being comparable to the exciton Bohr diameters [19]. As demonstrated from the single-particle spectroscopic characterizations, the perovskite NCs are featured with blinking-free photoluminescence (PL) [20], ultranarrow PL linewidth [20,21], coherent single-photon emission [21,22], and exciton fine-structure splitting [23–28]. These superior optical properties are gradually approaching those commonly possessed by epitaxial QDs, suggesting the emergence of a potent platform that might bridge the missing gap between these two important semiconductor nanostructures [29]. So far, the QCSE of perovskite NCs has been largely unexplored [30], the understanding of which will not only provide a better guidance for their optoelectronic performances in light-emitting diodes [31] and solar cells [32], but also extend the classical applications of colloidal NCs to the regime of quantum technologies.

Here we focus on single perovskite $CsPbI_3$ NCs, showing how their optical properties are modulated by an external electric field at the cryogenic temperature. For single excitons created by low-power laser excitation, the electric field can induce a blueshift in the PL peak to reveal the existence of a permanent dipole moment. Such a permanent dipole moment is theoretically proposed to arise from the surface-related stress, which could reduce the crystal symmetry by creating the hydrostatic strain. For single excitons and biexcitons created with high-power laser excitation, their fine energy-level structures can be simultaneously eliminated to create two cascaded decay channels with indistinguishable emission wavelengths but orthogonally linear polarizations.

According to a standard procedure [25], the $CsPbI_3$ NCs passivated with surface oleic acid and oleylamine ligands are synthesized with a cubic edge length of ~9.3 nm. For the optical measurements at 4 K, a single $CsPbI_3$ NC is placed between two electrodes and excited at 570 nm by a 5.6 MHz picosecond laser (see experimental details in the Supplemental Material [33]). In Fig. 1(a), we present an optical image of the excitation laser spot located between two nearby electrodes. In Fig. 1(b), we plot the PL spectrum measured for a single $CsPbI_3$ NC within the

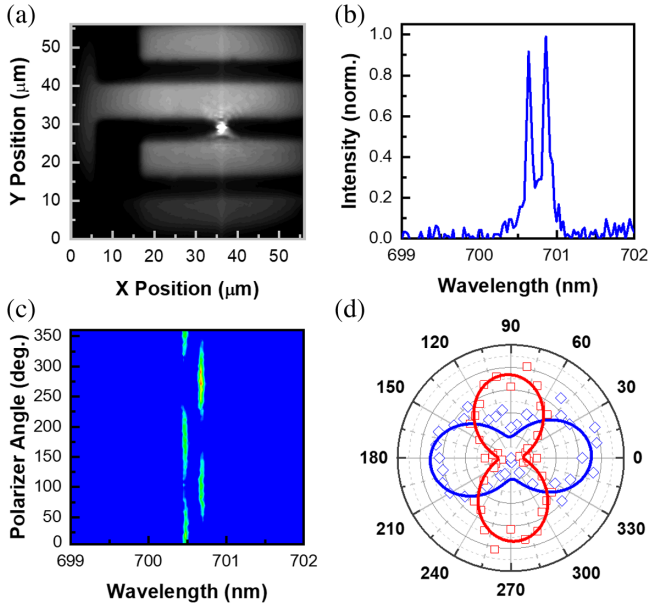

FIG. 1. (a) Optical image showing the excitation laser spot located between two nearby electrodes. (b) Doublet PL peaks measured for a single $CsPbI_3$ NC. (c) PL spectral image of this single $CsPbI_3$ NC showing PL intensity changes of the doublet peaks with the detection angles of the linear polarizer. (d) PL intensities of the doublet peaks each shown in a polar plot as a function of the linear polarizer angle. The blue (red) data points correspond to the PL peak shown in (c) with a high (low) energy.

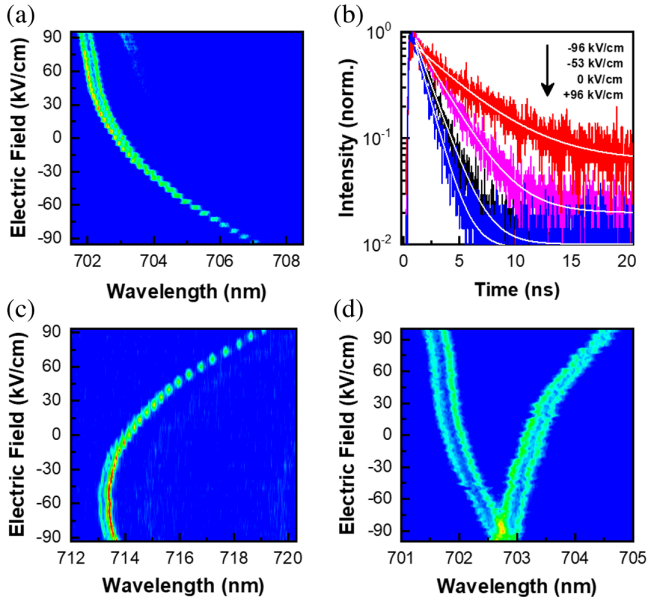

FIG. 2. (a) PL spectral image of a single $CsPbI_3$ NC showing the single-exciton peak shift as a function of the external electric field. (b) PL decay curves of this single $CsPbI_3$ NC measured at different electric fields and each fitted by a single-exponential function. (c) PL spectral image of another single $CsPbI_3$ NC showing the single-exciton peak shift as a function of the external electric field. (d) PL spectral image of two single $CsPbI_3$ NCs showing the crossover of their single-exciton peaks at about -90 kV/cm.

laser spot, which is consisted of doublet peaks with resolution-limited PL linewidths of ~ 100 μeV. As shown in the spectral image of Fig. 1(c), these doublet peaks possess anticorrelated changes in their PL intensities with the linear polarizer angles. In Fig. 1(d), the doublet PL intensities are each shown in a polar plot as a function of the polarizer angle, where the orthogonally linear polarizations confirm that they originate from the single-exciton fine-structure splitting [25].

Under an external electric field, the overall shifting trends of the doublet PL peaks are quite similar, so that we will denote them together as the single-exciton peak in the following discussions. As shown in Fig. 2(a) from the PL spectral image of a single $CsPbI_3$ NC excited at $\langle N \rangle = 0.1$, with $\langle N \rangle$ being the number of excitons created per pulse [20,25,34], the single-exciton peak shifts from ~ 702 to ~ 707 nm with the decreasing electric field from 96 to -96 kV/cm. In a conventional QCSE process, the exciton peak would show a redshift once a positive or negative electric field is applied [35]. However, this symmetric electric-field response would be modified if there exists a permanent dipole moment inside the semiconductor nanostructure. For this specific single $CsPbI_3$ NC shown in Fig. 2(a), the built-in electric field related to the permanent dipole moment has already caused a redshift in the single-exciton peak, which is shifted further to the red side with the decreasing electric field from 0 to -96 kV/cm. In contrast, when the electric field is increased from 0 to 96 kV/cm, the built-in electric field would be gradually canceled to cause a blueshift in the single-exciton peak. As shown in Fig. 2(b), the single-exciton PL lifetime increases from ~ 1.50, ~ 2.35, to ~ 4.37 ns with the decreasing electric fields from 0, -53, to -96 kV/cm, signifying a reduced overlap of the electron-hole wave functions [36,37]. On the other hand, the PL lifetime decreases from ~ 1.50 to ~ 1.21 ns with the increasing electric field from 0 to 96 kV/cm, owing to partial or complete compensation of the built-in electric field.

In Fig. 2(c), we plot the PL spectral image measured for another single $CsPbI_3$ NC at $\langle N \rangle = 0.1$, where the single-exciton peak shifts from ~ 719 to ~ 713 nm when the electric field is decreased from 96 to -60 kV/cm, and then it shifts slightly back to the red side when the electric field is further reduced to -96 kV/cm. These dramatically different responses to the electric field, as shown in Figs. 2(a) and 2(c), suggest that the permanent dipole moments of the two single $CsPbI_3$ NCs are oriented quite differently when they are spin coated onto the substrate. This random alignment has allowed us to easily tune the single-exciton peaks to the same position for two single $CsPbI_3$ NCs within the laser spot, as exemplified in Fig. 2(d) at the electric field around -90 kV/cm. In contrast to the single $CsPbI_3$ NCs

studied here, the single epitaxial QDs grown on the same substrate normally possess fixed directions in their single-exciton dipole moments [38]. To prepare wavelength-indistinguishable single-photon sources for the two-photon interference measurements, the two single epitaxial QDs had to be selected from different substrates with one of them being subjected to an external strain or electric field [39,40], which is lack of the tuning flexibility achieved here for the two single $CsPbI_3$ NCs.

With an external electric field (E), the induced change of the exciton recombination energy can be described as $\alpha E + \beta E^2$, where α and β are the permanent dipole moment and the exciton polarizability, respectively [41]. The α values for the two single $CsPbI_3$ NCs studied in Figs. 2(a) and 2(c) are fitted to be ~6.59 and ~7.73 Å, respectively, with the corresponding β values being ~451 and ~749 meV/(MV/cm)^2, respectively (see Fig. S1 in the Supplemental Material for the fitting curves [33]). Overall, the electric-field induced shifts of the single-exciton peaks have been measured for 52 single $CsPbI_3$ NCs (see Fig. S2 for the experimental results from six more single $CsPbI_3$ NCs [33]), whose fitted α and β values range from ~0.11–11.24 Å and ~108–1159 meV/(MV/cm)^2 with the averages of 3.74 ± 2.71 Å and 366 ± 234 meV/(MV/cm)^2, respectively (see Fig. S3 for the statistics [33]). Using the relationship of $E_0 = \alpha/(2\beta)$ [3,41], we can determine the projected component of the built-in electric field E_0 in the E direction, which ranges from ~0.8–387.6 kV/cm with an average of 64.35 ± 58.08 kV/cm (see Fig. S3 for the statistics [33]). Given the fact that the directions of E_0 and E may form a nonzero angle between each other, we infer that the real magnitude of E_0 could be even larger than the estimated value.

The existence of a permanent dipole moment, with the associated built-in electric field, has been previously attributed to different origins in semiconductor nanostructures. It was suggested that charge carriers trapped on or near the surface of a colloidal NC could cause a transient dipole moment [3,42,43]. However, we are focusing entirely on neutral single $CsPbI_3$ NCs, while the charging status can be otherwise easily detected by the appearance of a redshifted PL peak (see Fig. S4 in the Supplemental Material [33]). In epitaxial InAs QDs, the asymmetric shape and nonuniform composition could yield a permanent dipole moment, which would be further modified by the structural truncation [41,44–47]. This origin is also unapplicable to the perovskite $CsPbI_3$ NCs studied here, owing to their cubic shape and homogeneous ion distribution [19].

Because of lattice mismatch and the accompanied strain in the core-shell interface of colloidal NCs, it was speculated that a permanent dipole moment would be induced through the piezoelectric effect [48,49]. When assuming that there exists a nonzero surface stress in $CsPbI_3$, we would also expect an induced strain in the cubic NC relative to its bulk phase [50,51]. Based on first-principles calculations, it has been predicted that the strain can profoundly influence the electronic structures of perovskite $CsPbI_3$ [52]. If the crystal structure remains centrosymmetric, the strain origin of a permanent dipole moment should have been excluded in our case. However, this scenario would be deviated if the strain could reduce the crystal symmetry to a lower one. In fact, due to the polar nature of the noncentrosymmetric crystallographic lattice in colloidal CdSe NCs [53–56], a permanent dipole moment was previously probed from either dielectric dispersion [53] or transient birefringence [54] measurement. We thus propose that a spontaneous polarization P occurs as a result of the symmetry reduction under the surface-induced strain, the discontinuity of which at the surface then produces the built-in electric field and the permanent dipole moment in a single $CsPbI_3$ NC. As the macroscopic electrostatic field induced by the polarization is $E_0 = P/(\varepsilon_0 \varepsilon)$, the observed built-in electric field (e.g., ~387.6 kV/cm) corresponds to a polarization of ~0.9–2 μC/cm^2 with a dielectric constant ε of 23–60 for low-dimensional perovskites [57].

From our first-principles calculations for the elastic parameters of the bulk $CsPbI_3$ and the (001) surface in the cubic phase [58], the surface-induced strain is plotted in Fig. 3(a) as a function of L/a_0, where L is the NC edge length and a_0 is the bulk lattice constant (see theoretical calculations in the Supplemental Material [33]). With the decreasing L/a_0 from 20 to 5, the strain shows an increasing trend from ~0.05 to ~0.17%. We further calculate in Fig. 3(b) how the energies per cubic unit cell in the centrosymmetric and noncentrosymmetric cubic structures vary with the strain along the most favorable [001] direction, showing that the latter one should be more

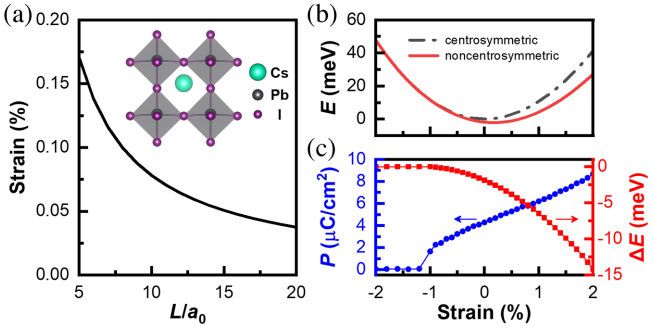

FIG. 3. (a) Surface-induced strain in a cubic $CsPbI_3$ NC plotted as a function of the edge length in unit of the lattice constant. The inset shows the noncentrosymmetric crystal structure of the cubic phase under the strain, which demonstrates displacement of the Cs ion relative to the I ions along the [001] direction. (b) The energies per cubic unit cell in the centrosymmetric and noncentrosymmetric structures as a function of the strain, where the unit-cell energy of the nonstrained centrosymmetric structure is set to zero as a reference. (c) Spontaneous polarization P in the noncentrosymmetric structure and its energy gain per cubic unit cell relative to the centrosymmetric structure, both plotted as a function of the strain.

stable when the strain is larger than a certain value. The corresponding energy gain of the symmetry reduction, together with the spontaneous polarization, are both plotted in Fig. 3(c) as a function of the strain. One can see that the magnitude of the polarization is around several $\mu C/cm^2$ and increases with the increasing tensile strain, suggesting that larger polarizations would be expected in smaller-sized NCs. On the other hand, due to the effect of depolarization fields, the measured polarization value should be smaller than what is shown in Fig. 3(c). Thus, our theoretical results are consistent with the experimental polarization values of $\sim$0.9–2 $\mu C/cm^2$.

Since it is also quite common for all-inorganic perovskite NCs to adopt an orthorhombic crystal phase [59], we additionally compare the relative stability of the centrosymmetric and noncentrosymmetric orthorhombic structures under different strains (see theoretical calculations and Fig. S5 in the Supplemental Material [33]). As in the case of the cubic phases, the centrosymmetric structure in the orthorhombic phase becomes unstable with respect to the noncentrosymmetric ones under sufficiently large strains, with the favorable polarization directions being along [001] and [011]. It should be noted that, whether a single $CsPbI_3$ NC is in the cubic or the orthorhombic phase, our theoretical model predicts the existence of a noncentrosymmetric structure that is intimately related to the built-in electric field. In a recent work [60], we have detected transversal-acoustic phonon modes that are size quantized in single $CsPbI_3$ NCs with the energies ranging from $\sim$150–180 μeV, which can be activated only when the material lacks of the inversion symmetry [61]. Moreover, right after the application or removal of an external electric field, we have observed relaxation behaviors in the single-exciton PL peaks of single $CsPbI_3$ NCs (see Fig. S6 in the Supplemental Material [33]), suggesting that the existence of a built-in electric field should signify the structural deviation from the original centrosymmetric phase.

The doublet PL peaks from single excitons in a single $CsPbI_3$ NC have been treated as a whole in the above discussions of electric-field responses. However, there still exists a delicate difference in their shifting rates to the blue and red sides. As can be seen in Figs. 2(a) and 2(c), the high-energy peak always shifts faster to the blue and red sides than the low-energy one, leading to a larger (smaller) fine-structure splitting at the shorter (longer) wavelength. Whenever the doublet PL peaks are being shifted to the red side with the changing electric field, they would eventually arrive at the same wavelength position [see Figs. 2(a) and 2(c)], which should reflect the ultimate limit for the spatial separation of the electron and hole wave functions in a single $CsPbI_3$ NC with the weak quantum confinement. In Fig. S7(a) [33], we plot the PL spectral image measured for another single $CsPbI_3$ NC excited at $\langle N\rangle = 0.1$, whose PL spectra extracted at five different electric fields are plotted in Fig. S7(b) [33]. The fine-structure splitting is estimated

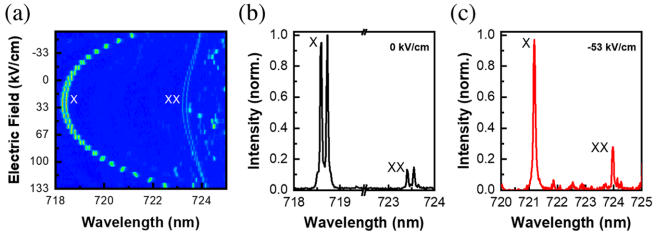

FIG. 4. (a) PL spectral image of a single $CsPbI_3$ NC showing the single-exciton (X) and biexciton (XX) peak shifts as a function of the external electric field. PL spectra measured for this single $CsPbI_3$ NC at the electric fields of (b) 0 and (c) -53 kV/cm, respectively.

to be $\sim$230 μeV at 0 kV/cm, and it increases to $\sim$509 and $\sim$743 μeV at the positive electric fields of 33 and 133 kV/cm, respectively. After the negative electric field has been applied, the fine-structure splitting is greatly shortened to $\sim$91 μeV at -33 kV/cm and it is almost completely removed at -67 kV/cm, resulting in a single peak with a PL linewidth of $\sim$137 μeV.

We next increase the laser power to set $\langle N\rangle = 1.0$ so that the PL responses of single excitons and biexcitons of a single $CsPbI_3$ NC can be studied together under an external electric field in Fig. 4(a). In Fig. 4(b), we plot the PL spectrum measured at 0 kV/cm, where the fine-structure splittings for the single excitons and biexcitons are both $\sim 338 \pm 20$ μeV. When the electric field is decreased to -53 kV/cm in Fig. 4(c), both single excitons and biexcitons now possess a single peak with a PL linewidth of $\sim$150 μeV (see Fig. S8 [33] for more PL spectra of this single $CsPbI_3$ NC measured at different electric fields). From the above observations (see Fig. S9 [33] for similar results of three more single $CsPbI_3$ NCs), it is feasible to generate polarization-entangled photon pairs from a single $CsPbI_3$ NC in future works. To accomplish this challenging goal, the system spectral resolution has to be optimized to be better than $\sim$20 μeV for a precise removal of the exciton fine-structure splitting, which is the narrowest PL linewidth currently available for single $CsPbBr_3$ [21] or $CsPbI_3$ [22,60] NCs.

To summarize, we have applied external electric fields to single perovskite $CsPbI_3$ NCs with a weak quantum confinement, showing that they can serve as a very sensitive nanomaterial for the electro-optical modulation applications. Meanwhile, the PL peak of a single $CsPbI_3$ NC demonstrates an asymmetric shift under the positive and negative electric fields, from which the existence of a permanent dipole moment can be deduced. This permanent dipole moment is proposed to originate from the surface stress that is capable of reducing the crystal symmetry by creating the hydrostatic strain, which should also be applicable to other semiconductor perovskites to influence their optical processes in practical optoelectronic devices. We have also shown that the external electric fields can be

employed to completely remove the fine-structure splittings for both single excitons and biexcitons, thus preparing a very fundamental ingredient for realizing polarization-entangled photon pairs measurement on single $CsPbI_3$ NCs. This achievement has marked the smooth transition of semiconductor colloidal NCs from ensemble optoelectronic devices to single-particle quantum technologies, with the associated advantages of facile synthesis, low cost, visible-wavelength emission and easy integration into various optical structures.

This work is supported by the National Key Research and Development Program of China (No. 2017YFA0303700 and No. 2019YFA0308700), the National Natural Science Foundation of China (No. 61974058 and No. 11974164), the Priority Academic Program Development of Jiangsu Higher Education Institutions, and the Open Project Program of Wuhan National Laboratory for Optoelectronics (No. 2018WNLOKF019).

[*]These authors contributed equally to this work.
[†]Corresponding author.
wxiaoyong@nju.edu.cn
[‡]Corresponding author.
djshu@nju.edu.cn
[§]Corresponding author.
mxiao@uark.edu

[1] D. A. B. Miller, D. S. Chemla, T. C. Damen, A. C. Gossard, W. Wiegmann, T. H. Wood, and C. A. Burrus, Phys. Rev. Lett. **53**, 2173 (1984).
[2] A. Högele, S. Seidl, M. Kroner, K. Karrai, R. J. Warburton, B. D. Gerardot, and P. M. Petroff, Phys. Rev. Lett. **93**, 217401 (2004).
[3] S. A. Empedocles and M. G. Bawendi, Science **278**, 2114 (1997).
[4] A. J. Bennett, M. A. Pooley, R. M. Stevenson, M. B. Ward, R. B. Patel, A. B. de la Giroday, N. Sköld, I. Farrer, C. A. Nicoll, D. A. Ritchie, and A. J. Shields, Nat. Phys. **6**, 947 (2010).
[5] M. Ghali, K. Ohtani, Y. Ohno, and H. Ohno, Nat. Commun. **3**, 661 (2012).
[6] H. Wang, H. Hu, T.-H. Chung, J. Qin, X. Yang, J.-P. Li, R.-Z. Liu, H.-S. Zhong, Y.-M. He, X. Ding, Y.-H. Deng, Q. Dai, Y.-H. Huo, S. Höfling, C.-Y. Lu, and J.-W. Pan, Phys. Rev. Lett. **122**, 113602 (2019).
[7] E. Menendez-Proupin and C. Trallero-Giner, Phys. Rev. B **69**, 125336 (2004).
[8] J. Müller, J. M. Lupton, P. G. Lagoudakis, F. Schindler, R. Koeppe, A. L. Rogach, J. Feldmann, D. V. Talapin, and H. Weller, Nano Lett. **5**, 2044 (2005).
[9] F. Vietmeyer, T. Tchelidze, V. Tsou, B. Janko, and M. Kuno, ACS Nano **6**, 9133 (2012).
[10] A. W. Achtstein, A. V. Prudnikau, M. V. Ermolenko, L. I. Gurinovich, S. V. Gaponenko, U. Woggon, A. V. Baranov, M. Y. Leonov, I. D. Rukhlenko, A. V. Fedorov, and M. V. Artemyev, ACS Nano **8**, 7678 (2014).
[11] R. Scott, A. W. Achtstein, A. V. Prudnikau, A. Antanovich, L. D. A. Siebbeles, M. Artemyev, and U. Woggon, Nano Lett. **16**, 6576 (2016).
[12] E. Rothenberg, M. Kazes, E. Shaviv, and U. Banin, Nano Lett. **5**, 1581 (2005).
[13] K. Becker, J. M. Lupton, J. Müller, A. L. Rogach, D. V. Talapin, H. Weller, and J. Feldmann, Nat. Mater. **5**, 777 (2006).
[14] H. Steinberg, O. Wolf, A. Faust, A. Salant, Y. Lilach, O. Millo, and U. Banin, Nano Lett. **10**, 2416 (2010).
[15] K. Park, Z. Deutsch, J. J. Li, D. Oron, and S. Weiss, ACS Nano **6**, 10013 (2012).
[16] O. Bar-Elli, D. Steinitz, G. Yang, R. Tenne, A. Ludwig, Y. Kuo, A. Triller, S. Weiss, and D. Oron, ACS Photonics **5**, 2860 (2018).
[17] R. M. Kraus, P. G. Lagoudakis, A. L. Rogach, D. V. Talapin, H. Weller, J. M. Lupton, and J. Feldmann, Phys. Rev. Lett. **98**, 017401 (2007).
[18] C. E. Rowland, K. Susumu, M. H. Stewart, E. Oh, A. J. Mäkinen, T. J. O'Shaughnessy, G. Kushto, M. A. Wolak, J. S. Erickson, A. L. Efros, A. L. Huston, and J. B. Delehanty, Nano Lett. **15**, 6848 (2015).
[19] L. Protesescu, S. Yakunin, M. I. Bodnarchuk, F. Krieg, R. Caputo, C. H. Hendon, R. X. Yang, A. Walsh, and M. V. Kovalenko, Nano Lett. **15**, 3692 (2015).
[20] F. Hu, C. Yin, H. Zhang, C. Sun, W. W. Yu, C. Zhang, X. Wang, Y. Zhang, and M. Xiao, Nano Lett. **16**, 6425 (2016).
[21] H. Utzat, W. Sun, A. E. K. Kaplan, F. Krieg, M. Ginterseder, B. Spokoyny, N. D. Klein, K. E. Shulenberger, C. F. Perkinson, M. V. Kovalenko, and M. G. Bawendi, Science **363**, 1068 (2019).
[22] Y. Lv, C. Yin, C. Zhang, W. W. Yu, X. Wang, Y. Zhang, and M. Xiao, Nano Lett. **19**, 4442 (2019).
[23] G. Rainò, G. Nedelcu, L. Protesescu, M. I. Bodnarchuk, M. V. Kovalenko, R. F. Mahrt, and T. Stöferle, ACS Nano **10**, 2485 (2016).
[24] M. Fu, P. Tamarat, H. Huang, J. Even, A. L. Rogach, and B. Lounis, Nano Lett. **17**, 2895 (2017).
[25] C. Yin, L. Chen, N. Song, Y. Lv, F. Hu, C. Sun, W. W. Yu, C. Zhang, X. Wang, Y. Zhang, and M. Xiao, Phys. Rev. Lett. **119**, 026401 (2017).
[26] M. Isarov, L. Z. Tan, M. I. Bodnarchuk, M. V. Kovalenko, A. M. Rappe, and E. Lifshitz, Nano Lett. **17**, 5020 (2017).
[27] M. A. Becker, R. Vaxenburg, G. Nedelcu, P. C. Sercel, A. Shabaev, M. J. Mehl, J. G. Michopoulos, S. G. Lambrakos, N. Bernstein, J. L. Lyons, T. Stoferle, R. F. Mahrt, M. V. Kovalenko, D. J. Norris, G. Raino, and A. L. Efros, Nature (London) **553**, 189 (2018).
[28] P. Tamarat, M. I. Bodnarchuk, J.-B. Trebbia, R. Erni, M. V. Kovalenko, J. Even, and B. Lounis, Nat. Mater. **18**, 717 (2019).
[29] M. Bayer, Ann. Phys. (Amsterdam) **531**, 1900039 (2019).
[30] D. K. Sharma, S. Hirata, V. Biju, and M. Vacha, ACS Nano **13**, 624 (2019).
[31] T. Chiba, Y. Hayashi, H. Ebe, K. Hoshi, J. Sato, S. Sato, Y.-J. Pu, S. Ohisa, and J. Kido, Nat. Photonics **12**, 681 (2018).
[32] A. Swarnkar, A. R. Marshall, E. M. Sanehira, B. D. Chernomordik, D. T. Moore, J. A. Christians, T. Chakrabarti, and J. M. Luther, Science **354**, 92 (2016).

[33] See Supplemental Material at http://link.aps.org/supplemental/10.1103/PhysRevLett.126.197403 for experimental details; theoretical calculations; fitting curves, and PL spectral images for the changes of single-exciton peaks with the electric fields; statistical distributions of the permanent dipole moments, exciton polarizabilities and built-in electric fields; PL spectral image of charged excitons; responses of single-exciton PL peaks with the application and removal of external electric fields; evolution of fine-structure splittings for single excitons and biexcitons with the electric fields.
[34] N. S. Makarov, S. Guo, O. Isaienko, W. Liu, I. Robel, and V. I. Klimov, Nano Lett. **16**, 2349 (2016).
[35] H. Gotoh, H. Kamada, H. Ando, and J. Temmyo, Appl. Phys. Lett. **76**, 867 (2000).
[36] B. Höfer, J. Zhang, J. Wildmann, E. Zallo, R. Trotta, F. Ding, A. Rastelli, and O. G. Schmidt, Appl. Phys. Lett. **110**, 151102 (2017).
[37] A. Passaseo, M. De Vittorio, M. T. Todaro, I. Tarantini, M. De Giorgi, R. Cingolani, A. Taurino, M. Catalano, A. Fiore, A. Markus, J. X. Chen, C. Paranthoen, U. Oesterle, and M. Ilegems, Appl. Phys. Lett. **82**, 3632 (2003).
[38] A. Muller, Q. Q. Wang, P. Bianucci, and C. K. Shih, Appl. Phys. Lett. **84**, 981 (2004).
[39] E. B. Flagg, A. Muller, S. V. Polyakov, A. Ling, A. Migdall, and G. S. Solomon, Phys. Rev. Lett. **104**, 137401 (2010).
[40] R. B. Patel, A. J. Bennett, I. Farrer, C. A. Nicoll, D. A. Ritchie, and A. J. Shields, Nat. Photonics **4**, 632 (2010).
[41] P. Jin, C. M. Li, Z. Y. Zhang, F. Q. Liu, Y. H. Chen, X. L. Ye, B. Xu, and Z. G. Wang, Appl. Phys. Lett. **85**, 2791 (2004).
[42] M. Shim and P. Guyot-Sionnest, J. Chem. Phys. **111**, 6955 (1999).
[43] S.-J. Park, S. Link, W. L. Miller, A. Gesquiere, and P. F. Barbara, Chem. Phys. **341**, 169 (2007).
[44] M. Grundmann, O. Stier, and D. Bimberg, Phys. Rev. B **52**, 11969 (1995).
[45] P. W. Fry, I. E. Itskevich, D. J. Mowbray, M. S. Skolnick, J. J. Finley, J. A. Barker, E. P. O'Reilly, L. R. Wilson, I. A. Larkin, P. A. Maksym, M. Hopkinson, M. Al-Khafaji, J. P. R. David, A. G. Cullis, G. Hill, and J. C. Clark, Phys. Rev. Lett. **84**, 733 (2000).
[46] J. A. Barker and E. P. O'Reilly, Phys. Rev. B **61**, 13840 (2000).
[47] Y. M. Park, Y. J. Park, J. D. Song, and J. I. Lee, Solid State Commun. **134**, 391 (2005).
[48] X. Peng, M. C. Schlamp, A. V. Kadavanich, and A. P. Alivisato, J. Am. Chem. Soc. **119**, 7019 (1997).
[49] N. Q. Huong and J. Birman, J. Chem. Phys. **108**, 1769 (1998).
[50] H. Ibach, Surf. Sci. Rep. **29**, 195 (1997).
[51] Q. Zhao, A. Hazarika, L. T. Schelhas, J. Liu, E. A. Gaulding, G. Li, M. Zhang, M. F. Toney, P. C. Sercel, and J. M. Luther, ACS Energy Lett. **5**, 238 (2020).
[52] C. Grote and R. F. Berger, J. Phys. Chem. C **119**, 22832 (2015).
[53] S. A. Blanton, R. L. Leheny, M. A. Hines, and P. Guyot-Sionnest, Phys. Rev. Lett. **79**, 865 (1997).
[54] L.-S. Li and A. P. Alivisatos, Phys. Rev. Lett. **90**, 097402 (2003).
[55] H. Zang, M. Cristea, X. Shen, M. Liu, F. Caminoa, and M. Cotlet, Nanoscale **7**, 14897 (2015).
[56] E. Rabani, J. Chem. Phys. **115**, 1493 (2001).
[57] D. Sapori, M. Kepenekian, L. Pedesseau, C. Katan, and J. Even, Nanoscale **8**, 6369 (2016).
[58] D.-J. Shu, S.-T. Ge, M. Wang, and N.-B. Ming, Phys. Rev. Lett. **101**, 116102 (2008).
[59] F. Bertolotti, L. Protesescu, M. V. Kovalenko, S. Yakunin, A. Cervellino, S. J. L. Billinge, M. W. Terban, J. S. Pedersen, N. Masciocchi, and A. Guagliardi, ACS Nano **11**, 3819 (2017).
[60] Y. Lv, C. Yin, C. Zhang, X. Wang, Z.-G. Yu, and M. Xiao, Nat. Commun. **12**, 2192 (2021).
[61] T. Takagahara, Phys. Rev. Lett. **71**, 3577 (1993).